

Correlations between structure and optical properties in Jahn–Teller Mn^{3+} fluorides: A study of TiMnF_4 and NaMnF_4 under pressure

Fernando Rodriguez^{a)} and Fernando Aguado

DCITIMAC, Facultad de Ciencias, Universidad de Cantabria, Santander 39005, Spain

(Received 30 December 2002; accepted 4 March 2003)

This work investigates the Jahn–Teller (JT) distortion in different Mn^{3+} fluoride series by optical absorption (OA) spectroscopy. The aim is to establish correlations between the local structure of the formed MnF_6^{3-} derived from x-ray diffraction and the JT splitting associated with the parent octahedral ${}^5E_g(3z^2-r^2, x^2-y^2)$ and ${}^5T_{2g}(xy, xz, yz)$ states, Δ_e and Δ_t , obtained from the OA spectrum. A salient feature is the linear relation exhibited by both Δ_e and Δ_t with the tetragonal coordinate Q_θ along the whole series. From these relations we derive suitable electron-ion coupling coefficients related to the 5E_g and ${}^5T_{2g}$ states whose values play a key role in the $e \otimes E$ and $e \otimes T$ JT theory, respectively. The results of these correlations are applied to investigate the structural variations undergone by the two-dimensional compounds NaMnF_4 and TiMnF_4 under pressure using OA spectroscopy. Interestingly, the analysis carried out is relevant since it provides useful information on the Mn^{3+} local structure, a task that is difficult to achieve using extended x-ray-absorption fine structure under pressure due to the high absorption of the diamond anvils. We conclude that the effect of pressure in NaMnF_4 is to reduce progressively the JT distortion of the complex, keeping its tetragonal symmetry. The pressure effects in TiMnF_4 are more drastic, leading to pressure-induced structural phase transitions of low symmetry. At variance with NaMnF_4 , the high-pressure Mn^{3+} local structure seems to have significant rhombic distortions. © 2003 American Institute of Physics. [DOI: 10.1063/1.1569847]

I. INTRODUCTION

The great variety of structures of Mn^{3+} compounds and the associated properties related to the Jahn–Teller (JT) effect of Mn^{3+} make these materials attractive for applications. They have received considerable attention in several fields: Solid-state lasers (Mn^{3+} -doped $\text{Y}_3\text{Al}_5\text{O}_{12}$) (Refs. 1–3), dichroism ($\text{Ti}_2\text{MnF}_5 \cdot \text{H}_2\text{O}$) (Ref. 4), transparent ferromagnets (CsMnF_4) (Refs. 5–8), colossal magnetoresistance ($\text{Sm}_{0.55}\text{Sr}_{0.45}\text{MnO}_3$) (Refs. 9–11), or metal-insulator transition (LaMnO_3) (Ref. 12) are examples of such an ample behavior.

Among these materials, Mn^{3+} fluorides present a wide variety of structural, optical, and magnetic properties, which have been studied extensively in order to establish structural correlations.^{13–20} It is well known that their crystallographic structure is strongly influenced by the chemical stoichiometry. Depending on the composition as $A_3\text{MnF}_6$, $A_2\text{MnF}_5$, or $A\text{MnF}_4$ (A : monovalent cation) the number of shared F^- ligands between MnF_6^{3-} units increases, leading to structural arrangements of different dimensionality. In $A_2\text{MnF}_5$ or $B\text{MnF}_5$ (B : divalent cation) MnF_6^{3-} is packed as $\text{MnF}_4\text{F}_{2/2}$ units, thus favoring the formation of one-dimensional (1D) chains with two axially shared F^- ligands. On the other hand, Na_2MnF_5 (Ref. 21) and $\text{Ti}_2\text{MnF}_5 \cdot \text{H}_2\text{O}$ (Ref. 22) are examples of 1D systems. $A\text{MnF}_4$ compounds tend to form layers of $[\text{MnF}_2\text{F}_{4/2}]$ units.^{23–25} The layer consists of JT

elongated $[\text{MnF}_2\text{F}_{4/2}]$ octahedra whose short equatorial ligand of a given complex acts as long axial ligand of the neighbor octahedron, thus leading to an antiferrodistortive (AF) structure which favors ferromagnetic exchange interaction between Mn–Mn nearest neighbors. CsMnF_4 (Ref. 8) and NaMnF_4 (Ref. 23) are examples of 2D systems. In $A_3\text{MnF}_6$ (or $AB\text{MnF}_6$), a network (hereafter called 0D) of isolated MnF_6^{3-} octahedra is formed.^{26–28} In all these cases, the MnF_6^{3-} octahedra exhibit an elongated D_{4h} distortion due to the JT effect of the Mn^{3+} with d^4 high-spin configuration. The JT distortion appears enhanced in low-dimensional systems by crystal anisotropy. Figure 1 illustrates the crystal structure of 0D, 1D, and 2D Mn^{3+} fluorides. Interestingly, the degree of JT distortion correlates with the crystal dimensionality as is shown in Table I for a complete compound series. For comparison purposes, we use the octahedron normal coordinates Q_i , which are more useful than the Mn–F distances for describing JT distortions.²⁹ Besides the average Mn–F distance, JT distortions which are related to the $e \otimes E$ JT, are commonly well described through the (Q_θ, Q_ϵ) normal coordinates representing tetragonal and rhombic distortions of MnF_6^{4-} , respectively. These modes can be expressed as a function of the axial and equatorial distances R_{ax} , R_{eq1} , and R_{eq2} , as described in Fig. 1. It is worth noting that aside the rhombic distortion, which is $Q_\epsilon \approx 0$, the tetragonal JT distortion has values of $Q_\theta \approx 0.2, 0.3,$ and 0.4 \AA for 0D, 1D, and 2D systems, respectively, along the fluoride series (Table I). This correlation provides an attractive way for exploring physical properties, which are

^{a)}Author to whom correspondence should be addressed. Electronic mail: rodrigu@unican.es

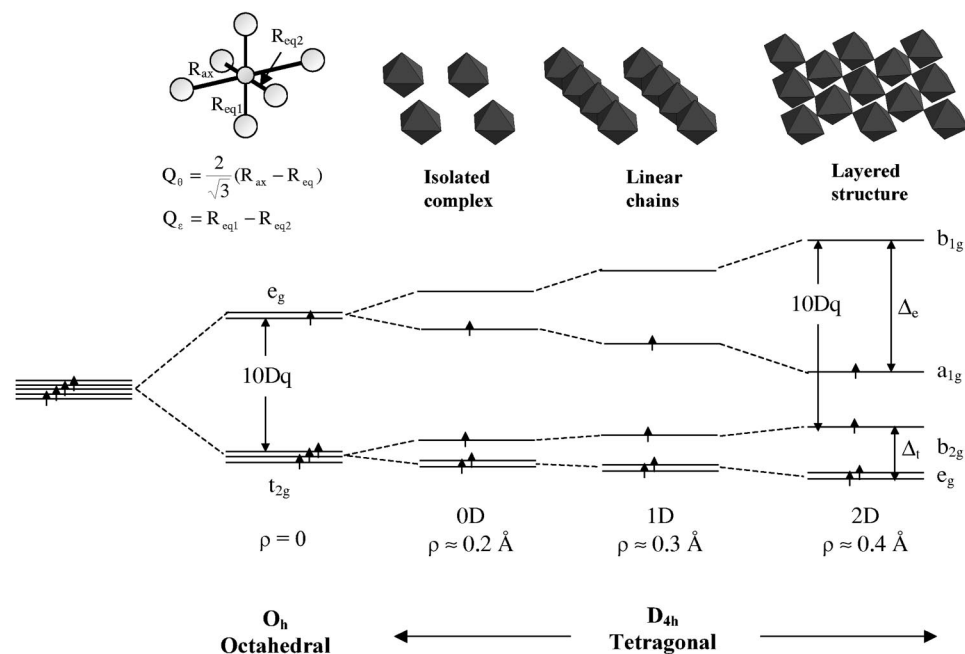


FIG. 1. Diagram of the d levels of Mn^{3+} for different dimensionality compounds. The upper part of the figure shows the 0D (isolated complex), 1D (linear chains), and 2D (layered compound) octahedral arrangements. Note the antiferrodistortive structure (2D) displayed by the corner-sharing MnF_6^{3-} octahedra. The relationships between the spectroscopic parameters and energy levels are also shown in the figure. A view of the elongated coordination of the MnF_6^{3-} complex, with the corresponding axial and equatorial Mn–F distances R_{ax} , R_{eq1} , and R_{eq2} is depicted on left top. The normal coordinates Q_θ and Q_ε representing the tetragonal and rhombic distortions, respectively, are given as a function of the three Mn–F distances.

strongly dependent on the local structure of Mn^{3+} , just by employing compounds of different dimensionality. Owing to this, the optical properties associated with electronic transitions involving crystal-field (CF) excitations within the $3d^4$ electron configuration constitute a paradigm.

In this work, we investigate the optical absorption (OA) spectra of several Mn^{3+} compounds displaying a wide vari-

ety of local structures in order to establish correlations between the CF and the local structure. This knowledge is important in order to get insight into the electron–ion coupling responsible for the JT effect as well as its associated energy strongly dependent on the complex distortion. For this purpose, we study Na_2MnF_5 - and $Tl_2MnF_5 \cdot H_2O$ -like 1D compounds and $NaMnF_4$ - and $TlMnF_4$ -like 2D representatives.

TABLE I. Structural and spectroscopic parameters for Mn^{3+} compounds of different dimensionality. E_1 , E_2 , and E_3 are the CF energies associated with transitions between electron orbitals $b_{1g}(x^2-y^2) \rightarrow a_{1g}(3z^2-r^2)$, $b_{1g}(x^2-y^2) \rightarrow b_{2g}(xy)$, and $b_{1g}(x^2-y^2) \rightarrow e_g(xz, yz)$, respectively. Δ_e and Δ_t are the tetragonal splitting defined as $\Delta_e = E_1$ and $\Delta_t = E_3 - E_2$. Crystal-field splitting $10Dq$ (eq) is obtained directly from E_2 . Here R_{ax} , R_{eq1} , and R_{eq2} are the equatorial and axial Mn–F distances of the MnF_6^{3-} complex. The normal coordinates Q_θ and Q_ε are related to these distances as $Q_\theta = (2/\sqrt{3})(R_{ax} - R_{eq})$ with $R_{eq} = \frac{1}{2}(R_{eq1} + R_{eq2})$ and $Q_\varepsilon = R_{eq1} - R_{eq2}$. The geometric average of both distortions is represented by $\rho = \sqrt{Q_\theta^2 + Q_\varepsilon^2}$. The average Mn–F distance (R_m) and the complex volume are also included. On the other hand, crystal parameters of these compounds (lattice parameters and space group) appear in the table.

Compound	E_3 (eV)	$E_2 = 10Dq$ (eV)	$E_1 = \Delta_e$ (eV)	$\Delta_t = E_3 - E_2$ (eV)	R_{ax} (\AA)	R_{eq1} (\AA)	R_{eq2} (\AA)	R_{eq} (\AA)	Q_θ (\AA)	Q_ε (\AA)	ρ (\AA)	R_m (\AA)	V_{oct} (\AA^3)	Space group	a (\AA)	b (\AA)
$K_2NaMnF_6^a$	2.418	2.170	1.116	0.248	2.060	1.860	0.231	...	0.231	1.927	2.376
$Na_3MnF_6^b$	2.380	2.182	1.041	0.198	2.018	1.862	1.897	1.880	0.160	0.035	0.164	1.926	2.376
$K_3MnF_6^a$	2.430	2.230	1.120	0.200
$(NH_4)_2MnF_5^c$	2.604	2.256	1.581	0.347	2.091	1.838	1.842	1.840	0.289	0.004	0.290	1.924	2.360	<i>Pnma</i>	6.200	7.940
$Na_2MnF_5^d$	2.604	2.232	1.550	0.372	2.103	1.829	1.872	1.851	0.291	0.043	0.288	1.935	2.400	<i>P21/c</i>	7.719	5.236
$K_2MnF_5^c$	2.653	2.325	1.500	0.329
$Tl_2MnF_5 \cdot H_2O^f$	2.579	2.170	1.451	0.409	2.082	1.818	1.845	1.832	0.289	0.027	0.290	1.915	2.328	<i>Cmcm</i>	9.688	8.002
$NH_4MnF_4^g$	2.752	2.281	1.822	0.471
$NaMnF_4^h$	2.817	2.263	1.915	0.554	2.167	1.869	1.808	1.839	0.379	0.061	0.383	1.948	2.441	<i>P21/c</i>	5.736	4.892
$KMnF_4^i$	2.765	2.269	1.909	0.496	2.155	1.870	1.800	1.835	0.370	0.070	0.376	1.942	2.418	<i>P21/a</i>	7.706	7.657
$CsMnF_4^i$	2.727	2.232	1.922	0.496	2.162	1.860	1.821	1.841	0.371	0.039	0.373	1.948	2.441	<i>P4/nmm</i>	7.944	7.944
$TlMnF_4^j$	2.737	2.233	1.824	0.504	2.146	1.861	1.776	1.819	0.378	0.085	0.387	1.928	2.364	<i>I2/a</i>	5.397	5.441
$TlMnF_4^k$	2.727	2.256	1.798	0.471	2.146	1.861	1.776	1.819	0.378	0.085	0.387	1.928	2.364	<i>I2/a</i>	5.397	5.441
$RbMnF_4^l$	2.789	2.294	1.922	0.496	2.154	1.882	1.805	1.844	0.358	0.077	0.366	1.947	2.439	<i>P21/a</i>	7.820	7.776

^aD. Oelkrug, Struct. Bonding **9**, 1 (1971).

^bReferences 13 and 28.

^cR. Sears and J. L. Hoard, J. Chem. Phys. **50**, 1066 (1969).

^dReference 35 and reference in footnote a.

^eT. S. Davis, J. P. Fackel, and M. J. Weeks, Inorg. Chem. **7**, 1994

^fReferences 4 and 22. 13.

^gW. Massa, Inorg. Nucl. Chem. Letters **13**, 253 (1977) and Ref. 13.

^hThis work and Ref. 23.

ⁱReferences 13 and 24.

^jThis work and Ref. 25.

^kReferences 13 and 25. (1968).

^lReferences 7 and 24.

The results will be compared with the optical spectrum of the 0D K_3MnF_6 .³⁰ The aim is to obtain local structural correlations from the OA spectra. The study is completed with a compound series of different dimensionality, whose structural and optical data are collected in Table I. The analysis carried out on these compounds has provided a general view on the JT effect of Mn³⁺.

The so-obtained correlations will be applied to study the variation of Mn³⁺ local structure induced by pressure in NaMnF₄ and TiMnF₄ from their CF spectra. A previous report on the pressure effect on NaMnF₄ using pressure spectroscopy revealed the CF spectrum as an efficient local probe to extract structural information around the Mn³⁺.³¹ This task is difficult to accomplish through extended x-ray absorption fine structure (EXAFS) due to the great absorption of the diamond anvils at the *K* edge of Mn ($E = 6.55$ keV).³² In addition, the variation of Mn–F distances as a function of pressure seems to be difficult to attain from x-ray diffraction (XRD) under pressure in $AMnF_4$ ($A = Cs, Na, Rb$) (Ref. 33) given that the local structural information must be extracted from intensity analysis. The reported XRD diagrams were not suitable for such a purpose.^{33–35} Therefore the search for alternative techniques being able to provide local-structure information is noteworthy.

The effects of pressure will be compared with the spectroscopic results derived from compound series (chemical pressure). As a salient result, we show that the pressure effect on the crystal and Mn³⁺ local structure is very similar to the chemical-pressure effects attained upon cation substitution—i.e., the replacement of Cs for Rb or Na in CsMnF₄.^{6,7,33} Although this result was already shown on the basis of space-group cell analysis,³³ we extend this study beyond the crystal structure to include the Mn³⁺ local structure. Interestingly, both chemical and hydrostatic pressure procedures have been used in this work for obtaining suitable values of the electron–ion coupling parameters that are relevant in the $e \otimes E$ JT theory.^{31,36}

II. EXPERIMENT

A. Synthesis and crystallographic structure of the investigated compounds

Single crystals of $Tl_2MnF_5 \cdot H_2O$, NaMnF₄, and TiMnF₄ were grown following the method reported elsewhere.^{22–25} Two different 1D compounds are investigated in this work. First, $Tl_2MnF_5 \cdot H_2O$ has an orthorhombic $Cmcm$ space group with lattice parameters $a = 9.688(2)$ Å, $b = 8.002(1)$ Å, and $c = 8.339(1)$ Å at room temperature. The structure consists of linear chains of transconnected $[MnF_4F_{2/2}]$ octahedra along the *c* direction, displaying nearly D_{4h} symmetry (Fig. 1). The long Mn–F distance is $R_{ax} = 2.082$ Å, and the equatorial ones are $R_{eq1} = 1.818$ Å and $R_{eq2} = 1.845$ Å. The Mn–F–Mn angle is 179.2° .²² Second, Na₂MnF₅ has a monoclinic $P2_1/c$ space group with the lattice parameters $a = 7.719(1)$ Å, $b = 5.236(1)$ Å, $c = 10.862(2)$ Å, and $\beta = 109.0^\circ$. Like in the previous case, the chain structure contains strings of corner-connected octahedra along the *c* direction. The Mn–F distances are $R_{ax} = 2.103$ Å, $R_{eq1} = 1.872$ Å, and $R_{eq2} = 1.829$ Å.³⁵

The NaMnF₄-layered compound is monoclinic ($P2_1/c$ space group, $Z = 2$) with lattice parameters $a = 5.736$ Å, $b = 4.892$ Å, $c = 5.748$ Å, and $\beta = 108.1^\circ$ at room temperature.²² The structure consists of layers of interconnected $[MnF_2F_{4/4}]^{3-}$ corner-sharing octahedra separated by Na ions. The octahedra display a D_{2h} symmetry (nearly D_{4h}) as a consequence of the JT effect and crystal anisotropy. The in-plane equatorial F ligand of one Mn acts as axial ligand of the nearest Mn, leading to the layered AF structure of Fig. 1. The Mn–F distances are $R_{ax} = 2.167$ Å, $R_{eq1} = 1.869$ Å, and $R_{eq2} = 1.808$ Å.²² The layered structure is the same for TiMnF₄, with tetragonal $Imam$ space group and lattice parameters $a = 5.397(2)$ Å, $b = 5.441(2)$ Å, and $c = 12.484(5)$ Å with $\beta = 90.2^\circ$. The Mn–F distances are $R_{ax} = 2.146$ Å, $R_{eq1} = 1.861$ Å, and $R_{eq2} = 1.776$ Å.²⁵ A complete structural data collection for the three different dimensional compound series is given in Table I.

B. Optical absorption spectra

The OA spectra of NaMnF₄ and TiMnF₄ under pressure were obtained using a specially designed spectrophotometer for working with microsamples. The monochromatic light in the UV–VIS–IR range was obtained by means of Spectra Pro-300i Acton Research Corporation Monochromator and suitable filters. The chopped light was detected with a Hamamatsu R-928 Phototube and a SR 830 lock-in amplifier. Details of the experimental setup are given elsewhere.³⁶ Pressure experiments were done in a DAC (Diamond Optics, Inc.) using single crystals of $150 \times 120 \times 60$ μm³. We used paraffin oil as pressure transmitting media in order to prevent oxidation. The pressure was measured through the ruby *R*-line shift. The ruby was excited with the 530.9-nm line of a coherent CR-500K Kr⁺-ion laser. The OA spectra for $Tl_2MnF_5 \cdot H_2O$ crystals ($1 \times 0.5 \times 0.2$ mm³) and pellets of Na₂MnF₅ were obtained from a Lambda 9 Perkin–Elmer spectrophotometer equipped with Glan–Taylor polarizing prisms.⁴

III. RESULTS

The OA spectra of NaMnF₄ and TiMnF₄ in the UV–VIS range at ambient conditions are shown in Fig. 2. These spectra as well as those for the AMnF₄ series basically consist of three broad intense bands. Besides there are additional sharp features whose absorption intensity strongly depends on the crystal dimensionality. The energy at the band maximum of the three broadbands, named E_1 , E_2 , and E_3 , for NaMnF₄ is 1.915, 2.263, and 2.817 eV, respectively. The energy state diagram together with the corresponding crystal and local structures is shown in Fig. 1. For the 2D isomorphous TiMnF₄, these bands are located at 1.824, 2.233, and 2.737 eV, respectively. The two sharp features correspond to spin-flip transitions between quintuplet and triplet spin states. In contrast to the broadbands the sharp-peak energy

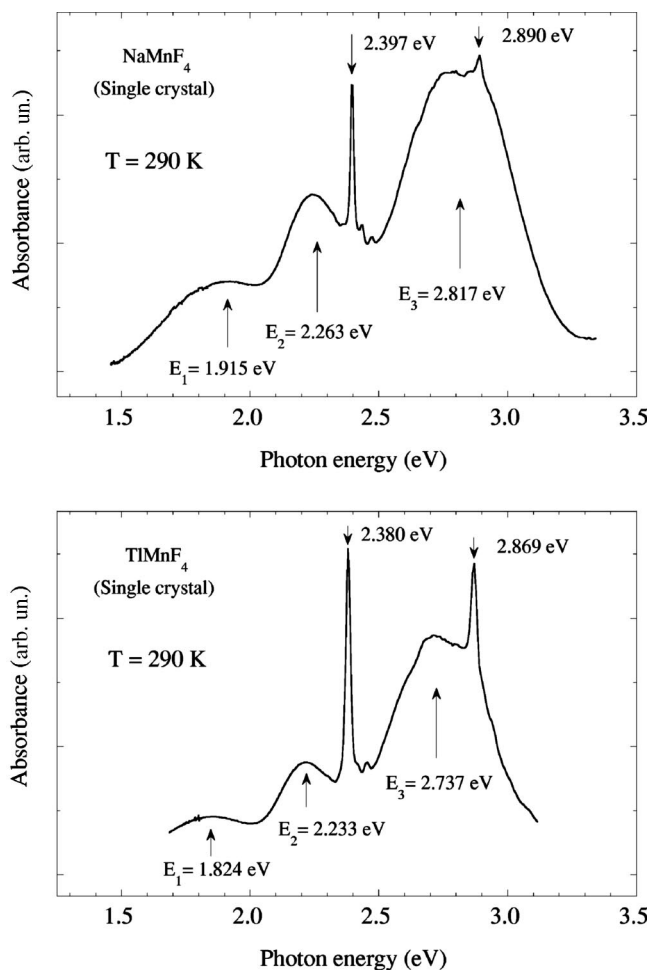


FIG. 2. Optical absorption spectra of NaMnF_4 and TiMnF_4 single crystals at ambient conditions. Note that both spectra corresponding to 2D compounds are quite similar. The energy of the narrow and broad bands are also indicated by arrows.

depends slightly on the crystal structure as is shown in Fig. 2. In fact, they are located at 2.397 and 2.890 eV in NaMnF_4 and 2.380 and 2.869 eV in TiMnF_4 .

The OA spectrum of the 1D systems $\text{Ti}_2\text{MnF}_5 \cdot \text{H}_2\text{O}$ and Na_2MnF_5 are shown in Fig. 3. Both spectra present also three broadbands but located at 1.451, 2.170, and 2.579 eV in $\text{Ti}_2\text{MnF}_5 \cdot \text{H}_2\text{O}$ and at 1.55, 2.23, and 2.62 eV in Na_2MnF_5 . In single crystals of $\text{Ti}_2\text{MnF}_5 \cdot \text{H}_2\text{O}$ the three bands are strongly polarized as can be seen by comparing OA taken with light polarized along the chain (π spectrum) or perpendicular to it (σ spectrum). This behavior is responsible for the marked dichroism exhibited by the 1D systems in comparison to 2D or 0D compounds.⁴ The analysis of the polarized spectra and their variation with temperature, performed elsewhere,⁴ clearly points out that the three transitions correspond to ED transitions from the ${}^5B_{1g}$ ground state to the ${}^5A_{1g}$, ${}^5B_{2g}$, and ${}^5E_{1g}$ excited states, respectively, such as is shown in Figs. 2 and 3. Furthermore, the variation of the band intensity with temperature indicates that odd-parity vibrations mainly enable the ED transition mechanism. Hence the oscillator strength associated with broad-band transitions increases with temperature, at variance with

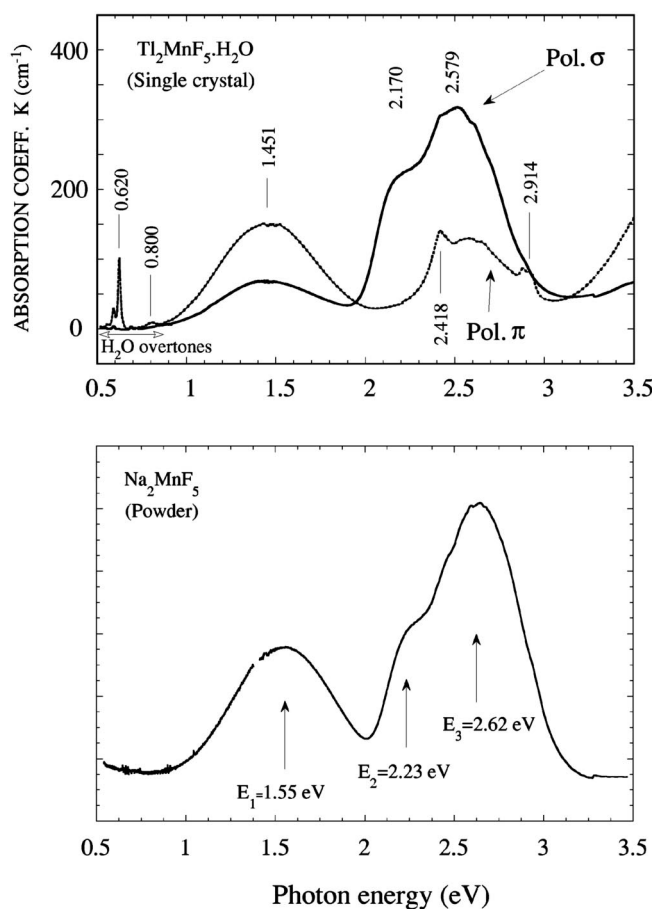


FIG. 3. Optical absorption spectra of $\text{Ti}_2\text{MnF}_5 \cdot \text{H}_2\text{O}$ (single crystal) in π and σ polarizations and Na_2MnF_5 (powder) at ambient conditions. The strong polarization character exhibited by $\text{Ti}_2\text{MnF}_5 \cdot \text{H}_2\text{O}$ illustrates the marked pleochroism of these 1D compounds.

spin-flip transitions, whose intensity is fully activated by the exchange mechanism.^{4,36}

The OA spectra of 1D and 2D compounds are compared with the 0D K_3MnF_6 in Fig. 4. This latter compound shows three absorption bands, which are located at 1.12, 2.23, and 2.43 eV. Note that the first band is shifted to lower energies with respect to 1D and 2D systems, while the other two bands show a rather important overlap, making it difficult to obtain the corresponding band maxima. In Fig. 4 we have plotted three characteristic spectra according to the JT distortion of the associated MnF_6^{3-} complex given by the coordinate $\rho = \sqrt{Q_e^2 + Q_\theta^2} \approx Q_\theta$ (Table I). Interestingly, the transition energy of the first OA band increases linearly with the complex distortion. This correlation provides a useful procedure to obtain structural information about the MnF_6^{3-} complex or the crystal dimensionality through OA.^{31,36}

IV. ANALYSIS AND DISCUSSION

A. Jahn–Teller distortion: Perturbative model

The OA spectra of all Mn^{3+} fluorides are very similar. The energy of the CF bands can be explained to a great extent within the MnF_6^{3-} complex, due to the marked local character and the high ionicity of F^- . Within a complex

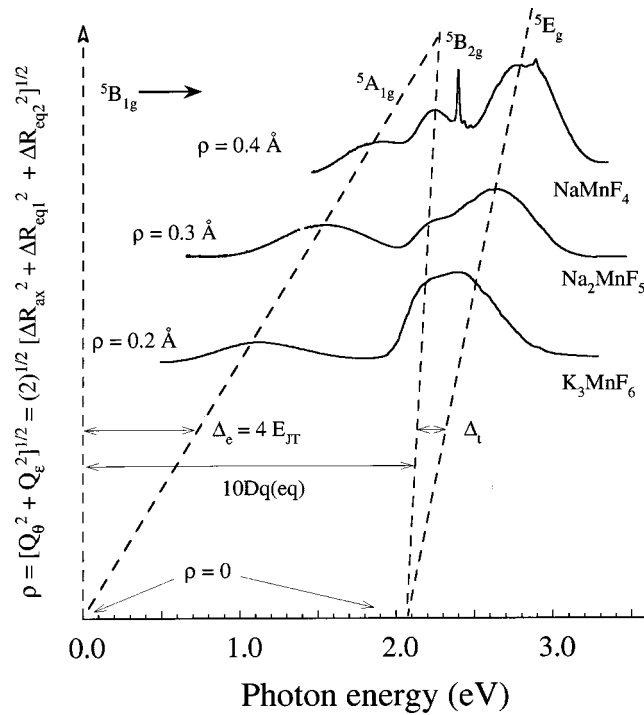


FIG. 4. Optical absorption spectra of 0D, 1D, and 2D Mn³⁺ compounds. The three bands shift to lower energies as dimensionality decreases. Note that the tetragonal splitting Δ_e and Δ_t increase with ρ showing a nearly linear dependence. An O_h symmetry yielding splitting closure is produced for $\rho=0$. Note that the complex distortion (ρ) increases with the crystal dimensionality.

framework for MnF₆³⁻, the CF energy diagram mainly relies on the type and degree of JT distortion. The use of compound series of different dimensionality is advantageous for this study since it provides an ample variety of geometries for MnF₆³⁻ (Table I).

For small deviations of the octahedral symmetry, the relation between the CF energy and the complex geometry can be easily derived within a perturbative scheme.²⁹ On the assumption that the complex distortion is either tetragonal or rhombic, what is the usual case for JT–Mn³⁺ fluorides, then the perturbed Hamiltonian can be described as a function of the octahedral e_g and a_{1g} normal coordinates as

$$\begin{aligned}
 H &= H_{O_h} + \Delta H \\
 &= H_{O_h} + \left(\frac{\partial H}{\partial Q_{a_{1g}}} \right)_{Q_\varepsilon = Q_\theta = 0} Q_{a_{1g}} \\
 &\quad + \left(\frac{\partial H}{\partial Q_\theta} \right)_{Q_{a_{1g}} = Q_\varepsilon = 0} Q_\theta + \left(\frac{\partial H}{\partial Q_\varepsilon} \right)_{Q_{a_{1g}} = Q_\theta = 0} Q_\varepsilon. \quad (1)
 \end{aligned}$$

The normal coordinates are defined as follows:

$$\begin{aligned}
 Q_{a_{1g}} &= \sqrt{6} \left[\frac{1}{3} (R_{ax} + R_{eq1} + R_{eq2}) - R_0 \right], \\
 Q_\theta &= \frac{2}{\sqrt{3}} (R_{ax} - R_{eq}), \quad Q_\varepsilon = R_{eq2} - R_{eq1},
 \end{aligned}$$

where $R_{eq} = \frac{1}{2}(R_{eq1} + R_{eq2})$ is the average of the two equatorial distances and R_0 is the unperturbed average Mn–F dis-

tance. At the same time it is very convenient to introduce the parameter $\rho = \sqrt{Q_\theta^2 + Q_\varepsilon^2}$ since it plays a key role in the $e \otimes E$ JT theory.^{29,37,38}

The representation matrices of ΔH for the parent octahedral ${}^5T_{2g}(xy, xz, yz)$ and ${}^5E_g(3z^2 - r^2, x^2 - y^2)$ states are then given by

$$\begin{aligned}
 \langle \Delta H \rangle &= -4C \begin{pmatrix} 1 & 0 & 0 \\ 0 & 1 & 0 \\ 0 & 0 & 1 \end{pmatrix} Q_{a_{1g}} \\
 &\quad + \frac{1}{\sqrt{6}} A_1^t \begin{pmatrix} 2Q_\theta & 0 & 0 \\ 0 & -Q_\theta + \sqrt{3}Q_\varepsilon & 0 \\ 0 & 0 & -Q_\theta - \sqrt{3}Q_\varepsilon \end{pmatrix}
 \end{aligned}$$

for ${}^5T_{2g}$ and

$$\langle \Delta H \rangle = 6C \begin{pmatrix} 1 & 0 \\ 0 & 1 \end{pmatrix} Q_{a_{1g}} + \frac{1}{2} A_1^e \begin{pmatrix} -Q_\theta & Q_\varepsilon \\ Q_\varepsilon & Q_\theta \end{pmatrix} \quad (2)$$

for 5E_g .

The coupling parameter C is related to the CF parameter $10Dq$ by

$$C = \frac{1}{\sqrt{6}} \left(\frac{\partial 10Dq}{\partial R} \right),$$

where R is the average Mn–F distance and A_i^j ($i = e_g, t_{2g}$) is the JT electron–ion coupling coefficient, which is quite different for the e_g and t_{2g} one-electron wave functions (or analogously the ${}^5T_{2g}$ and 5E_g states).

Within this perturbative scheme, the CF energy for each state is then given by

$$\begin{aligned}
 E({}^5B_{1g}) &= -6(Dq + CQ_{a_{1g}}) - \frac{1}{2} A_1^e \sqrt{Q_\theta^2 + Q_\varepsilon^2}, \\
 E({}^5A_{1g}) &= -6(Dq + CQ_{a_{1g}}) + \frac{1}{2} A_1^e \sqrt{Q_\theta^2 + Q_\varepsilon^2}, \\
 E({}^5B_{2g}) &= 4(Dq + CQ_{a_{1g}}) - \frac{2}{\sqrt{6}} A_1^t Q_\theta, \\
 E({}^5E_g) &= 4(Dq + CQ_{a_{1g}}) + \frac{1}{\sqrt{6}} A_1^t (Q_\theta \pm \sqrt{3}Q_\varepsilon).
 \end{aligned} \quad (3)$$

Note that the state energy has an opposite sign than the one-electron energy. In these equations we used the D_{4h} notation, i.e., $Q_\varepsilon = 0$, so that $3d$ levels split into four CF levels. If we consider an additional rhombic distortion beyond D_{4h} , then the degenerate 5E_g state splits into ${}^5B_{2g}$ and ${}^5B_{3g}$, and the corresponding band appears split in the OA spectrum. Thus the transition energy of each band in D_{4h} is given by

$$\begin{aligned}
 E_1 &= E({}^5A_{1g}) - E({}^5B_{1g}) = A_1^e Q_\theta = K_e \rho, \\
 E_2 &= E({}^5B_{2g}) - E({}^5B_{1g}) \\
 &= 10(Dq + CQ_{a_{1g}}) - \left(\frac{2}{\sqrt{6}} A_1^t - \frac{1}{2} A_1^e \right) Q_\theta \\
 &= 10Dq(eq), \quad (4)
 \end{aligned}$$

$$E_3 = E(^5E_g) - E(^5B_{1g}) \\ = 10(Dq + CQ_{a_{1g}}) + \left(\frac{1}{\sqrt{6}}A_1^t + \frac{1}{2}A_1^e \right) Q_\theta.$$

Within CF theory,^{39,40} the transition energy E_2 depends on R_{eq} as the octahedral $10Dq$ parameter;⁴⁰ hence, it is usually named as $10Dq(\text{eq})$. In case of a rhombic distortion, Q_θ must be replaced for ρ in E_1 , and E_3 splits into two states E_3^1 and E_3^2 , whose respective energies are

$$E_3^1 = E_3(D_{4h}) + \frac{1}{\sqrt{2}}A_1^t Q_\varepsilon, \quad (5)$$

$$E_3^2 = E_3(D_{4h}) - \frac{1}{\sqrt{2}}A_1^t Q_\varepsilon.$$

It is worthwhile noting that the tetragonal splitting of the octahedral e_g and t_{2g} levels, Δ_e and Δ_t , respectively, can be obtained directly from the OA spectrum as $\Delta_e = E_1$ and $\Delta_t = E_3 - E_2$. Within a perturbed- D_{4h} scheme, the two splitting can be written as $\Delta_e = E_1 = K_e Q_\theta$ and $\Delta_t = E_3 - E_2 = K_t Q_\theta$, where the proportionality constants are related to the electron-ion coupling coefficients by $K_e = A_1^e$ and $K_t = \sqrt{\frac{3}{2}}A_1^t$, respectively. In case of rhombic symmetry, Q_ε can be derived from the splitting of the 5E_g state as $\Delta_{\text{rhomb}} = E_3^1 - E_3^2 = \sqrt{2}A_1^t Q_\varepsilon$. The so-defined parameters are shown in Fig. 1.

Within the $e \otimes E$ JT framework, the electron-ion coupling between the $E(3z^2 - r^2, x^2 - y^2)$ states and $e_g(\theta, \varepsilon)$ vibrations in O_h symmetry yields a coordination equilibrium coordinate given by $\rho = A_1^e / 2k_e$,³⁷⁻³⁹ where k_e is the vibrational force constant. Note that A_1^e as defined in Eq. (2) is one-half the corresponding linear coupling constant employed elsewhere.^{37,38} The corresponding energy is given by

$$E_\pm = \pm \frac{1}{2}A_1^e \rho + \frac{1}{2}k_e \rho^2. \quad (6)$$

The \pm refers to the B_{1g} and A_{1g} states in D_{4h} and an appropriate combination of both states in D_{2h} . The B_{1g} stabilization energy is just the JT energy, which is given within this scheme by $E_{\text{JT}} = -\frac{1}{4}A_1^e \rho$. The energy difference between B_{1g} and A_{1g} gives directly the Δ_e splitting

$$\Delta_e = E_+ - E_- = A_1^e \rho = \frac{(A_1^e)^2}{2k_e} = 4E_{\text{JT}}. \quad (7)$$

Interestingly, OA can provide valuable information on the electron-ion coupling constants as well as the JT energy, since $E_1 = \Delta_e = 4E_{\text{JT}}$. In addition, the three compound series studied here are suitable for structural correlations since the corresponding OA spectra offer a direct characterization of the tetragonal and rhombic distortion, which are useful for understanding the $e \otimes E$ JT effect in Mn^{3+} systems. Furthermore, OA can be used as an efficient probe to explore structural distortions induced by either hydrostatic pressure or chemical pressure.

B. Absorption spectra: Influence of complex distortion

Throughout this work, we perform an analysis of the OA spectra along Mn^{3+} fluoride series on the basis of the MnF_6^{3-} complex with an axially elongated D_{4h} symmetry, since this is the usual coordination geometry displayed by most systems (Table I). The small rhombic distortion exhibited by some complexes will be treated as a perturbation of the D_{4h} symmetry. The spectrum series shown in Figs. 2 and 3, as well as data of Table I, support this view.

For all investigated compounds, we observe three broadbands that correspond to the $^5B_{1g} \rightarrow ^5\Gamma_i$, electron transitions with $\Gamma_i = A_{1g}$, B_{2g} , and E_g in order of increasing energy. This band assignment has been previously reported for the researched compounds in the present work.^{4,36}

The influence of dimensionality in the CF spectrum is illustrated in Fig. 4, by comparing spectra of 0D, 1D, and 2D systems. The absorption background is displaced along the vertical axis according to the complex distortion, ρ . The variation of $\Delta_e = E_1$ and $\Delta_t = E_3 - E_2$ is noteworthy. Both increase with the complex distortion and exhibit a linear behavior.

The JT energy for the investigated compounds is 0.39 and 0.36 eV for Na_2MnF_5 and $\text{Ti}_2\text{MnF}_5 \cdot \text{H}_2\text{O}$, respectively, whereas it is 0.48 and 0.46 eV for the 2D NaMnF_4 and TiMnF_4 . Consequently, E_{JT} as well as the Δ_t increases with complex distortion. This correlation is achieved not only for these compounds, but also for the compound series given in Table I.

A relevant feature is the usefulness of E_2 to explore variations of the equatorial Mn-F distance R_{eq} upon structural distortions. Given that E_2 depends only on R_{eq} , it provides a direct measurement of R_{eq} provided that we know the R_{eq} dependence of $10Dq(\text{eq})$. In this way, a dependence as $10Dq(\text{eq}) = A R_{\text{eq}}^{-n}$ with $n=5$ is found theoretical from the CF model.⁴⁰ Values between 4 and 5 have been attained for transition-metal complexes involving trivalent and divalent ions by either optical spectroscopy^{4,41,42} or calculations.⁴³⁻⁴⁵ This procedure has been exploited to derive the variation of R_{eq} in NaMnF_4 under pressure from OA.⁴⁶

C. Structural correlations for MnF_6^{3-}

The influence of the MnF_6^{3-} structure on the CF states is clearly evidenced in the OA spectra of different dimensionality compounds (Fig. 4). Table I gives the structural properties of the $A_3\text{MnF}_6$, $A_2\text{MnF}_5$, and $A\text{MnF}_4$ compounds series together with the corresponding transition energies and associated parameters deduced from their OA spectrum. Figure 5 shows different correlations between Δ_e and Δ_t and the structural parameters ρ and Q_θ as well as between $10Dq(\text{eq})$ and R_{eq} . As established elsewhere,³¹ both Δ_e and Δ_t increase linearly with Q_θ . The observed ratio $\Delta_e / \Delta_t \sim 4$ indicates a larger contribution to the splitting of the parent 5E_g and $^5T_{2g}$ octahedral states from the σ -bonding interaction of the e_g orbitals than from the π -bonding interactions due to the t_{2g} orbitals.^{4,47,48} It must be remarked that the variation of Δ_e with ρ , or Q_θ , provides similar values of the electron-ion coupling due to the strong

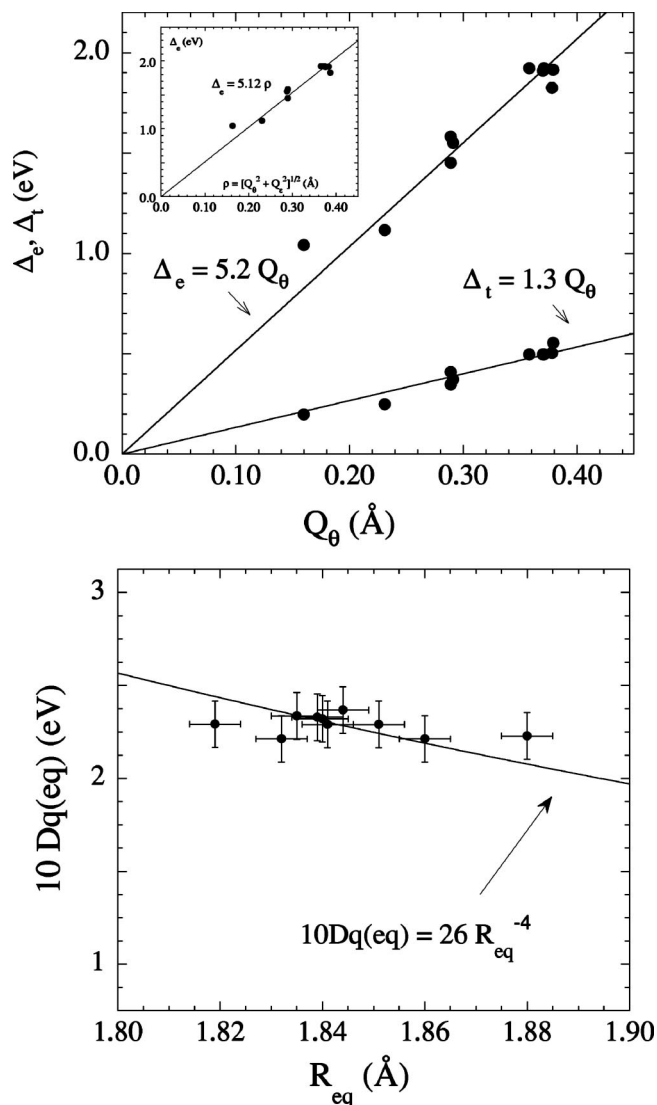


FIG. 5. Top: structural correlation between the tetragonal splitting Δ_e and Δ_t and the normal coordinate Q_θ . The inset shows the relation between Δ_θ and ρ . Note that it is quite similar to Q_θ for all Mn^{3+} compounds according to their nearly D_{4h} symmetry. Bottom: Variation of E_2 with R_{eq} along the compound series. The solid line represents the variation given by the equation $E_2 = A R_{\text{eq}}^{-4}$.

tetragonal character of JT complex in all compounds: $Q_e \approx 0$. The least-squares linear equation derived from the variation of Δ_e and Δ_t with Q_θ is $\Delta_e = K_e Q_\theta$ for the O_h e_g orbitals and $\Delta_t = K_t Q_\theta$ for the t_{2g} orbitals, with $K_e = 5.2 \text{ eV \AA}^{-1}$ and $K_t = 1.3 \text{ eV \AA}^{-1}$. It means that the electron–ion coupling constant defined in Eqs. (2) and (7) is $A_1^e = K_e = 5.2 \text{ eV \AA}^{-1}$ for the 5E_g state, whereas it is $A_1^t = \sqrt{\frac{2}{3}} K_t = 1.1 \text{ eV \AA}^{-1}$ for the ${}^5T_{2g}$ state. Concerning the ${}^5B_{1g} \rightarrow {}^5B_{2g}$ transition, Fig. 5 shows the variation of E_2 with R_{eq} along the compounds series. On the assumption of a R_{eq} dependence of $10Dq(\text{eq})$ as $10Dq(\text{eq}) = A/R_{\text{eq}}^n$, we are not able to derive any precise value of the n exponent from the plot of Fig. 5 due to data dispersion. However, the variation is consistent with a variation as R_{eq}^{-4} according to calculations performed on MnF_6^{3-} complexes.⁴⁹

The observed linear dependences of the spectroscopic parameters justify the assumed linear approximation as well

as the complex model for describing the CF electron structure of Mn^{3+} fluorides. However, it must be pointed out that this model does not apply on dealing with complex vibrations given that both the associated normal coordinates and their frequencies strongly depend on the neighboring ions beyond the first coordination sphere. Hence the influence of the crystal structure must be taken into consideration.

D. Variations of the crystal-field spectra of 2D compounds under pressure

Figure 6 shows the variation of the OA spectrum of NaMnF_4 and TiMnF_4 with pressure in the 0–10 GPa range. It must be noted that the evolution of each spectrum with pressure is very different. Whilst the variation of NaMnF_4 is progressive, maintaining the nearly tetragonal structure of OA bands in the whole pressure range, TiMnF_4 behaves distinctly depending on the pressure. Pressure effects on the OA spectrum of the former compound were explained on the basis of D_{4h} local-structure changes.^{31,46} The main conclusion is that the JT distortion of MnF_6^{3-} does not change significantly upon pressure. In fact, the hypothetical disappearance of the JT effect yielding $Q_\theta \approx 0$, should induce closure of the splitting of the octahedral 5E_g and ${}^5T_{2g}$ states: $\Delta_e = 0$ and $\Delta_t = 0$. On the contrary, we observe that both Δ_e and Δ_t increase 0.032 and 0.161 eV, respectively, from ambient pressure to 10 GPa. Consequently, we deduced that the MnF_6^{3-} volume reduces anisotropically with pressure. Both Mn–F distances R_{ax} and R_{eq} reduce with pressure, but the axial–distance variation is twice the equatorial distance, $\Delta R_{\text{ax}} \approx 2\Delta R_{\text{eq}}$, thus leading to a decrease of the JT distortion.

The situation for the thallium compound is rather different. Figures 6(b) and 7(b) show the variation of the OA spectrum and the transition energy of CF bands with pressure, respectively. A drastic change of the transition energy for each band is observed at about 1.5 and 3.2 GPa [Fig. 7(b)]. Between these two values, an important splitting of the tetragonal 5E_g state is clearly observed. Although the associated transition energy and splitting are difficult to determine due to the strong overlap, this feature likely indicates the presence of pressure-induced rhombic distortions. The complex band structure exhibited by the CF spectrum at high-pressure rules out any suitable analysis in terms of the corresponding structure variation of MnF_6^{3-} with pressure. However, the observed pressure dependence of the transition energy suggests the occurrence of pressure-induced structural phase transition at $P_{C1} = 1.5$ GPa and $P_{C2} = 3.2$ GPa. According to the phase diagram of the AMnF_4 crystal family,³³ we expect the high-pressure phase to be monoclinic. The local coordination geometry for MnF_6^{3-} that can be deduced from CF in this phase likely suggests a marked rhomboedral structure. The associated distortion should be stronger than the rhombic distortion exhibited by MnF_6^{3-} in monoclinic phases, whose value is $Q_e < 0.16 \text{ \AA}$. This upper Q_e limit corresponds to the highest value found among fluorides—i.e., the monoclinic $P21/a$ phase of RbMnF_4 (Table I). If we take a splitting of the ${}^5B_{1g} \rightarrow {}^5E_g$ band from the OA spectrum at 1.5 GPa of $\Delta_{\text{rhomb}} \approx 0.3 \text{ eV}$ [Fig. 6(b)], then the estimated rhombic distortion, following the struc-

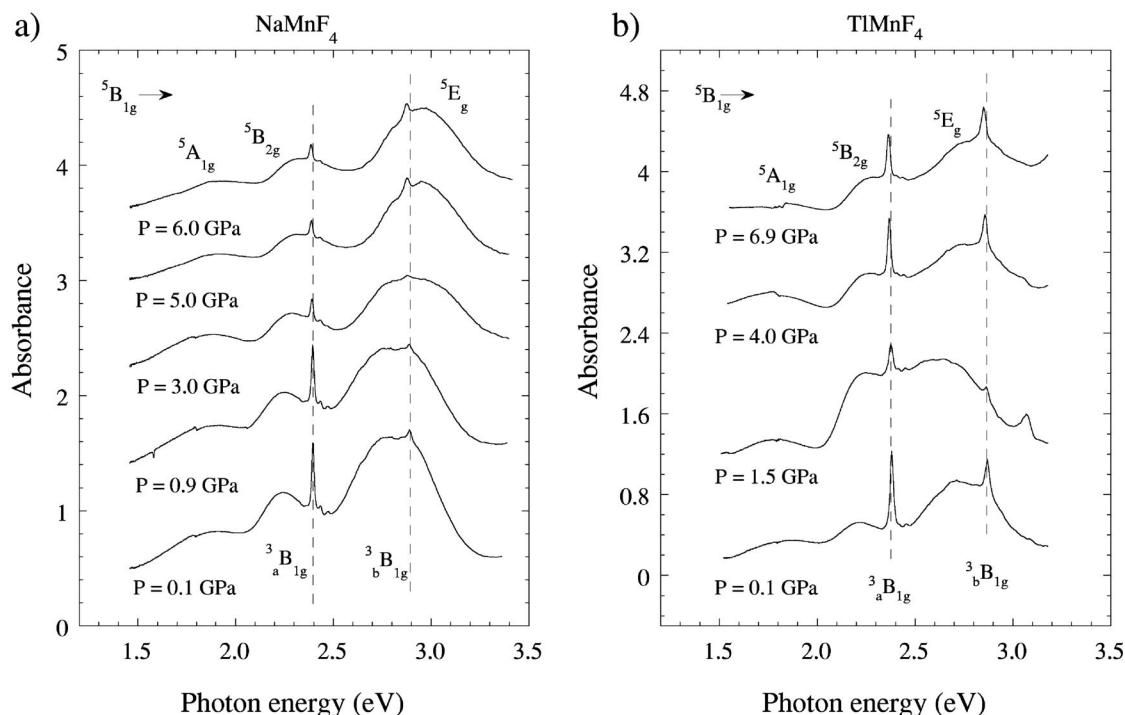


FIG. 6. Optical absorption spectra of the NaMnF₄ (a) and TiMnF₄ (b) single crystal and their variation with pressure. Dashed lines denote the position of the triplet peaks. Band assignment corresponds to the D_{4h} symmetry.

tural correlation established in Fig. 5, is $Q_\epsilon \approx \Delta_{\text{rhomb}} / \sqrt{2} A'_1 = 0.3/1.5 = 0.2 \text{ \AA}$. This estimate confirms that the MnF₆³⁻ rhombic distortion in the high-pressure phase of TiMnF₄ is bigger than in any other fluoride crystal (Table I).

The proposed model deserves verification through XRD experiments under pressure in order to support the present findings. Work along this line is currently in progress.

V. CONCLUSIONS

We have established correlations between the JT distortion around Mn³⁺ ions in fluorides and the tetragonal and rhombic splitting, which can be obtained through OA spec-

troscopy. The electron-ion coupling coefficients for the ${}^5E_g(3z^2 - r^2, x^2 - y^2)$ and ${}^5T_{2g}(xy, xz, yz)$ states have been determined through the linear dependence of the tetragonal parameters Δ_e and Δ_t with the normal-mode coordinate Q_θ along compound series of different dimensionality. The established correlations enabled us to develop a methodology for obtaining suitable information on the structural variations undergone by these Mn³⁺ systems either under hydrostatic pressure or varying the composition (chemical pressure). The method was applied to explore the structural transformations induced by the pressure in NaMnF₄ and TiMnF₄, both exhibiting a rather different behavior under pressure. While NaMnF₄ partially reduces the JT distortion, but preserving

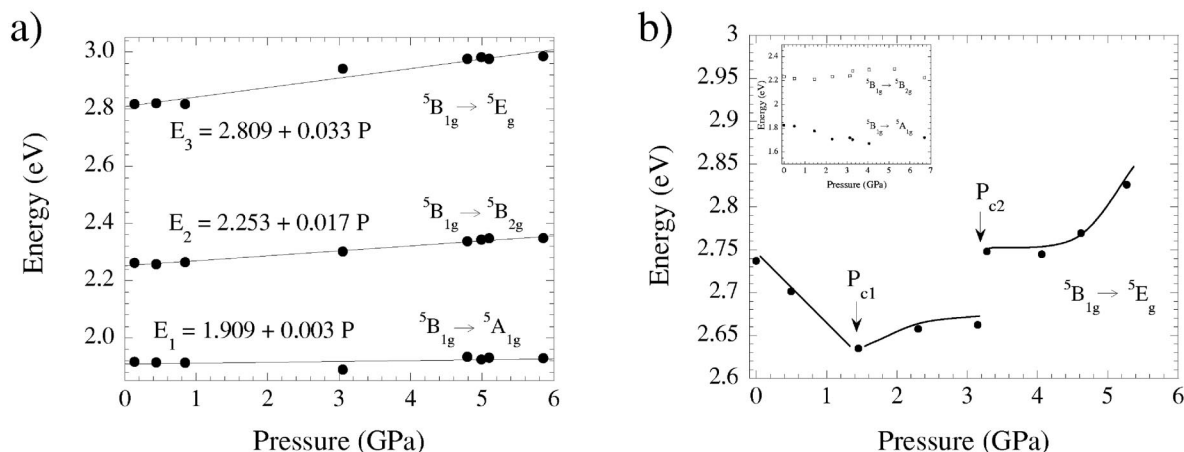


FIG. 7. Variation of the transition energy for the three bands E_1 , E_2 , and E_3 for NaMnF₄ (a) and TiMnF₄ (b) with pressure. For NaMnF₄, the energy varies linearly with pressure, whereas for TiMnF₄ it shows abrupt changes at 1.5 and 3.2 GPa. The complex band structure exhibited by this compound at high pressure reflects low-symmetry distortions, likely due to pressure-induced phase transitions.

its nearly tetragonal distortion upon pressure, TIMnF₄ experiences phase transformations with pressure that involve important local distortions of rhombic symmetry.

ACKNOWLEDGMENTS

The authors thank Professor Núñez for providing us with Mn³⁺ fluorides. F.A. is indebted to the Ministerio de Ciencia y Tecnología (MCyT) for a FPI research grant (Ref. No. FP99, Project No. PB98-0190). This work was financed by the Spanish MCyT (Project No. BFM2001-0695) and the Vicerrectorado de Investigación of the University of Cantabria.

- ¹K. Petermann and G. Huber, *J. Lumin.* **31/32**, 71 (1984).
- ²S. Kück, S. Hartung, S. Hurling, K. Petermann, and G. Huber, *Phys. Rev. B* **57**, 2203 (1998).
- ³S. Kück, S. Hartung, S. Hurling, and K. Petermann, *Laser Phys.* **8**, 206 (1998).
- ⁴F. Rodriguez, P. Nuñez, and M. C. Marco de Lucas, *J. Solid State Chem.* **110**, 370 (1994).
- ⁵M. C. Moron, F. Palacio, S. M. Clark, and A. Paduan-Filho, *Phys. Rev. B* **51**, 8660 (1995).
- ⁶F. Palacio and M. C. Moron, in *Research Frontiers in Magnetochemistry*, edited by C. J. O'Connor (World Scientific, Singapore, 1993).
- ⁷M. C. Moron, F. Palacio, and J. Rodriguez-Carvajal, *J. Phys.: Condens. Matter* **5**, 4509 (1993).
- ⁸W. Massa and J. Steiner, *J. Solid State Chem.* **32**, 137 (1980).
- ⁹M. R. Ibarra, P. A. Algarabel, C. Marquina, J. Blasco, and J. Garcia, *Phys. Rev. Lett.* **75**, 3541 (1995).
- ¹⁰J. M. de Teresa, M. R. Ibarra, J. Blasco *et al.*, *Phys. Rev. B* **54**, 1187 (1996).
- ¹¹J. Blasco, J. Garcia, J. M. de Teresa, M. R. Ibarra, J. Perez, P. A. Algarabel, C. Marquina, and C. Ritter, *Phys. Rev. B* **55**, 8905 (1997).
- ¹²I. Loa, P. Adler, A. Grzechnik, K. Syassen, U. Schwarz, M. Hanfland, G. Kh. Rozenberg, P. Gorodetsky, and M. P. Pasternak, *Phys. Rev. Lett.* **87**, 125 501 (2001).
- ¹³P. Kohler, W. Massa, D. Reinen, B. Hoffman, and R. Hoppe, *Z. Anorg. Allg. Chem.* **446**, 131 (1978).
- ¹⁴A. Tressaud and J. M. Dance, *Struct. Bonding (Berlin)* **52**, 87 (1982).
- ¹⁵W. Massa and D. Babel, *Chem. Rev.* **88**, 275 (1988).
- ¹⁶J. Pebler, W. Massa, H. Lass, and B. J. Ziegler, *J. Solid State Chem.* **71**, 87 (1987).
- ¹⁷P. Nuñez, J. Darriet, P. Bukovec, A. Tressaud, and P. Hagenmuller, *Mater. Res. Bull.* **22**, 661 (1987).
- ¹⁸F. Palacio, M. Andres, C. Esteban-Calderon, M. Martinez-Ripoll, and S. Garcia Blanco, *J. Solid State Chem.* **76**, 33 (1988).
- ¹⁹F. Palacio, M. Andres, J. Rodriguez-Carvajal, and J. Pannetier, *J. Phys.: Condens. Matter* **3**, 2340 (1991).
- ²⁰W. Massa and V. Burk, *Z. Anorg. Allg. Chem.* **516**, 119 (1984).
- ²¹W. Massa, *Acta Crystallogr., Sect. C: Cryst. Struct. Commun.* **42**, 644 (1986).
- ²²P. Nuñez, A. Tressaud, J. Darriet *et al.*, *Inorg. Chem.* **31**, 770 (1992).
- ²³M. Molinier, W. Massa, S. Khairoun, A. Tressaud, and J. L. Soubeyroux, *Z. Naturforsch. B* **46**, 1669 (1991).
- ²⁴M. Molinier and W. Massa, *Z. Naturforsch. B* **47**, 783 (1992).
- ²⁵P. Nuñez, A. Tressaud, J. Grannec, P. Hagenmuller, W. Massa, D. Babel, A. Boireau, and J. L. Soubeyroux, *Z. Anorg. Allg. Chem.* **609**, 71 (1992).
- ²⁶D. Babel, *Z. Anorg. Allg. Chem.* **336**, 200 (1965).
- ²⁷G. C. Allen, G. A. M. El-Sharkawy, and K. D. Warren, *Inorg. Chem.* **11**, 2538 (1971).
- ²⁸U. Englich, W. Massa, and A. Tressaud, *Acta Crystallogr., Sect. C: Cryst. Struct. Commun.* **48**, 6 (1992).
- ²⁹R. Valiente and F. Rodriguez, *Phys. Rev. B* **60**, 9423 (1999).
- ³⁰D. Oelkrug, *Ber. Bunsenges. Phys. Chem.* **70**, 736 (1966).
- ³¹F. Aguado, F. Rodriguez, and P. Nuñez, *High Press. Res.* **22**, 121 (2002).
- ³²F. Rodriguez, M. C. Marco De Lucas, C. Prieto, M. Verdaguer, and H. U. Güdel, *J. Phys. Chem. Solids* **56**, 995 (1995).
- ³³F. Palacio, M. C. Moron, and S. M. Clark, *Phys. Rev. B* **54**, 7052 (1996).
- ³⁴S. Carlson, Y. Xu, U. Halenius, and R. Norrestam, *Inorg. Chem.* **37**, 1486 (1998).
- ³⁵S. Carlson, Y. Xu, and R. Norrestam, *Z. Kristallogr.* **214**, 269 (1999).
- ³⁶F. Aguado, Graduate thesis, University of Cantabria, 2002.
- ³⁷D. Reinen and M. Atanasov, *Magn. Reson. Rev.* **15**, 167 (1991).
- ³⁸M. A. Hitchman, *Comments Inorg. Chem.* **15**, 197 (1994).
- ³⁹J. S. Griffith, *The Theory of Transition Metal Ions* (Cambridge University Press, Cambridge, England, 1980).
- ⁴⁰A. B. P. Lever, *Inorganic Electronic Spectroscopy* (Elsevier, Amsterdam, 1984).
- ⁴¹F. Rodriguez and M. Moreno, *J. Chem. Phys.* **84**, 692 (1986).
- ⁴²F. Rodriguez, M. Moreno, A. Tressaud, and J. P. Chaminade, *Cryst. Lattice Defects Amorphous Mater.* **16**, 221 (1987).
- ⁴³A. M. Woods, R. S. Sinkovits, and R. H. Bartram, *J. Phys. Chem. Solids* **55**, 91 (1994).
- ⁴⁴M. Moreno, J. A. Aramburu, and M. T. Barriuso, *Phys. Rev. B* **56**, 14423 (1997).
- ⁴⁵J. A. Aramburu, J. I. Paredes, M. T. Barriuso, and M. Moreno, *Phys. Rev. B* **61**, 6525 (2000).
- ⁴⁶F. Aguado, F. Rodriguez, and P. Nuñez (unpublished).
- ⁴⁷M. J. Riley, L. Dubicki, G. Moran, E. R. Krausz, and I. Yamada, *Chem. Phys.* **145**, 363 (1990).
- ⁴⁸D. Reinen, G. Steffen, M. A. Hitchman *et al.*, *Chem. Phys.* **155**, 117 (1991).
- ⁴⁹J. I. Paredes, Graduate thesis, University of Cantabria, 1996.